buildings

Article

Seismic Damage Assessment for Isolated Buildings with a Substructure Method

Lina Guo [1,2,3,4], Yong Ding [1,4,5,*] and Yifei Zhang [5]

1 Key Laboratory of Earthquake Disaster Mitigation of the Ministry of Emergency Management, Harbin 150000, China
2 College of Water Conservancy and Civil Engineering, Northeast Agricultural University, Harbin 150038, China
3 Traffic Safety and Control Lab in Hebei Province, Shijiazhuang 050000, China
4 Institute of Engineering Mechanics, China Earthquake Administration, Harbin 150080, China
5 School of Civil Engineering, Harbin Institute of Technology, Harbin 150090, China
* Correspondence: dingyong@hit.edu.cn

Abstract: A seismic damage detection method for isolated buildings is proposed based on substructure identification with incomplete contaminated measurements. A concept of a pseudo substructure with virtual conditions is constructed for the proof of the proposed substructure identification method. This identification method is implemented in a two-stage procedure. The interface forces of the target substructure are identified in the first stage and the parameter of the target substructure is updated in the second stage, which can enable the parameter identification of substructures with unknown input. Two computational methods are also proposed to improve the two-stage identification algorithm. A sub-time zone identification method is utilized to reduce the computation effort and the simultaneous identification of the unknown force and initial structural responses is presented in the first-stage identification for a general case in practical engineering. Numerical studies of a shear frame with nonlinear base isolation subject to earthquake ground motion are investigated to validate the proposed seismic damage detection method. A fourteen-storey concrete shear wall building with a two-storey steel frame on top connected by isolation is studied experimentally with shaking table tests to further validate the proposed method. The shear wall structure is taken as the target substructure for damage assessment. The interface force and parameter of the concrete shear wall building are estimated with the proposed method. Results from both the numerical simulations and laboratory tests indicate that the proposed method can estimate seismic isolated structures and detect damage effectively based on only a few accelerometers. It is also demonstrated that the parameter identification results based on the structure response measurement during the earthquake are more accurate than the identification with post-earthquake structural response measurement.

Keywords: substructure; isolation structure; damage detection; force identification; shaking table test

Citation: Guo, L.; Ding, Y.; Zhang, Y. Seismic Damage Assessment for Isolated Buildings with a Substructure Method. *Buildings* **2022**, *12*, 1185. https://doi.org/10.3390/buildings12081185

Academic Editors: Jiulin Bai, Wei Guo and Junxian Zhao

Received: 18 June 2022
Accepted: 25 July 2022
Published: 8 August 2022

1. Introduction

Structural seismic damage estimation is a major component of the function in a structural health monitoring system, which contributes to the seismic resilience. A large-scale structural system may have complex boundary conditions and uncertainties due to the discreteness of components in structures and variability in the material properties. Models on the boundary conditions and any innovative structural vibration control device for seismic protection in a large-scale civil structure may not be accurate. The identification accuracy of the superstructure, as the substructure of the whole structural system, may depend on the simulation results of the boundary conditions.

In the past few decades, many methods have been developed for structural health monitoring, structural parameter identification, and damage detection. There are review papers providing a detailed summary on the vibration-based damage identification methods [1–3]. These methods can be broadly classified into three categories: (1) time domain methods, (2) frequency-domain, and (3) time-frequency domain methods [1–4]. The methods in the frequency domain [5] include the peak picking method, methods with the transfer function, frequency response function, frequency domain decomposition, and eigensystem realization algorithm (ERA), etc. with tools in the frequency domain such as transfer function and modal parameters such as natural frequencies, mode shapes, mode shape curvature, flexibility matrices, mode strain energy [6–8], etc. Methods in the time domain include the Ibrahim time domain method, least-squares complex exponential method, and ERA methods. With measurements of the structure in the time domain, the location and severity of the local structural damage can be detected [9]. Mixed time and frequency domain techniques [4], such as the short-time Fourier transform, empirical mode decomposition, and wavelets, have also been applied to identify the linear time-variant and time-invariant systems.

The structural model updating method with the structural response sensitivity has been investigated and applied extensively to damage detection. The sensitivity matrix of the response with respect to the structural parameters is derived to locate and quantify the damage. It has been demonstrated that as few as a single sensor can accurately locate the damage with the sensitivity of the response [10,11]. A new damage identification approach has been proposed by Law [12] and local damage was identified through a substructure method. However, the literature on the structural response sensitivity method did not consider the influence of the coupling of the sensitivity matrices of the response and the interface force with respect to the structural parameters [13]. Additionally, they did not consider the nonlinear component in the structural system.

The performance of buildings with isolation subjected to strong earthquake excitations has been increasingly investigated. Numerous studies have been conducted on the seismic performance of base or inter-storey isolated structures. Most of the previous studies focused on the response of the isolation system or the response of the summation of the superstructure and the isolation system [14–17] while fewer studies have investigated the seismic condition evaluation and damage detection of this kind of structure. Considering the in situ calibration of the elastomeric bearings method with low cost, the nanoindentation test has been proposed as a promising tool for the isolation layer for the seismic isolated structure [18,19], which could also contribute to the superstructure's identification.

The substructural synthesis method has been applied to investigate complicated structures since the 1960s [20]. A large structural system can be divided into smaller substructures for separate analysis with a reduced number of unknowns [21–25]. The condensation method can also be applied to the structural dynamic analysis [26,27], but information from the condensed finite element model may not always match information from the original finite element model. However, the force identification in the first stage is always time-consuming work. Furthermore, the initial state of the structural response is commonly unknown and non-zero in practice. Target substructure identification with sensitivity matrix may be adversely influenced by the model error of the other substructures. There may some identification errors due to the errors in the structural time histories without considering the structural initial response. As the references mentioned above, a suitable application of the time-domain substructure identification method and computational efficiency should be developed, which is also the objectives of this study. There are also some modern computing methods that have been applied in classification, identification, and, especially, seismic vulnerability and fragility/damage assessment [28–31]. These series methods do not require the finite element model of structures and can be applied in areas with a high density of earthquakes while it works differently from damage detection by a structural health monitoring system, which can conduct comprehensive analysis with the damage detection results from measurement data and vulnerability analysis.

The substructure identification method is suitable for the identification of superstructures in seismically isolated buildings. The substructure identification method is firstly theoretically proved with the time domain response sensitivity with respect to the parameter in this study and then applied to the damage detection of seismically isolated buildings with an unknown initial structural response, including structural displacement, velocity, and acceleration. A new concept of a pseudo substructure with virtual boundary conditions is presented for the proof process, which was not found in previous study. The main structural system in a seismically isolated building can be divided into two substructures. One substructure is above the isolation layer while another substructure is below the isolation layer. The two substructures interact with each other via the isolation layer and the interaction force is unknown. A two-stage identification procedure is proposed in this process. With the substructure identification method, the interface forces can be identified in the state space in the first stage and the local damage is detected in the second stage. Two new computational methods are proposed to improve the first-stage identification. A sub-time zone force identification method in the first stage is proposed to improve the computation efficiency of the force identification. Additionally, a method of simultaneous identification of the interface force and the initial response on all DOFs of the structural system is illustrated to take into account the practical problem in engineering application. An adaptive Tikhonov regularization method is applied iteratively [32] with an adaptive limit to identify the damage extent [33], which improves the convergent property in practical application. The results of the numerical simulation of the shear frame with isolation and shaking table test of an inter-storey isolation structure are shown to be accurate even with measurement noise, an unknown initial structural response, and model errors.

2. Dynamic Responses for Substructures

The equation of motion of an N degrees-of-freedom (DOFs) damped structural system subject to base excitation and general external force can be represented as:

$$\mathbf{M}\ddot{\mathbf{x}} + f(\mathbf{x}, \dot{\mathbf{x}}) = -\mathbf{MG}\ddot{\mathbf{x}}_g + \mathbf{LF} \tag{1}$$

where $\mathbf{M}$ is the mass matrix and $f(\mathbf{x}, \dot{\mathbf{x}})$ denotes the summation of the damping force and restoring force, which may be nonlinear function. $\ddot{\mathbf{x}}_g$ represents the ground acceleration, $\mathbf{G}$ is the location matrix of the earthquake force, $\mathbf{F}$ denotes the vector of external excitation forces on the structure, and $\mathbf{L}$ is the mapping matrix for the external force $\mathbf{F}$. $\ddot{\mathbf{x}}$, $\dot{\mathbf{x}}$, and $\mathbf{x}$ are the vectors of acceleration, velocity, and displacement, respectively, of the structural system. Figure 1 shows a structural system with inter-storey isolation, which may behave nonlinearly during an earthquake or other extreme excitation. The main structural system, as shown in Figure 1, can be divided into two substructures as a summation of the substructure above the isolation and the substructure below, which may include the support and the soil mass surrounding the support. The equation of motion of each target substructure needs to include the interaction with the remaining part of the structural system [13]. The equation of motion for the substructure can be represented as:

$$\mathbf{M}_{ss}\ddot{\mathbf{x}}_s + \mathbf{C}_{ss}\dot{\mathbf{x}}_s + \mathbf{K}_{ss}\mathbf{x}_s = -(\mathbf{MG})_s\ddot{\mathbf{x}}_g + \mathbf{L}_s\mathbf{F}_s + \mathbf{F}_{in} \tag{2}$$

where $\mathbf{C}_{ss}$ and $\mathbf{K}_{ss}$ are the damping and stiffness matrices of the target substructure, respectively. The Rayleigh damping model is assumed in this paper as $\mathbf{C} = a_1\mathbf{M} + a_2\mathbf{K}$. $\mathbf{F}_{in}$ denotes the set of interface forces between the two substructures, the subscript s denotes the substructure above the isolation, and the subscript r denotes the substructure that is below the isolation. Subscripts sr and rs denote the interface DOFs of the substructures. Only in the linear structure, the interface forces can be accurately represented by $-(\mathbf{M}_{sr}\ddot{\mathbf{x}}_r + \mathbf{C}_{sr}\dot{\mathbf{x}}_r + \mathbf{K}_{sr}\mathbf{x}_r)$. In general cases, the interface force cannot be accurately represented. This is because finite element modeling of the interface is always difficult to achieve, or the interface forces may be a nonlinear function of the responses.

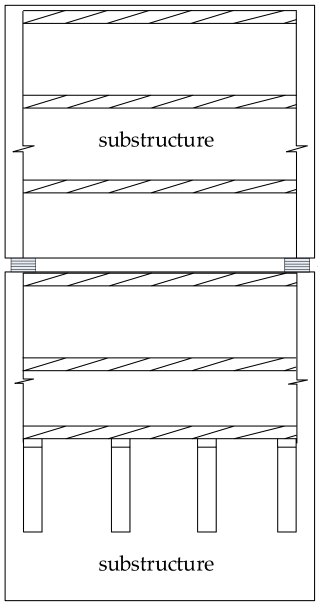

Figure 1. Configuration of the seismically isolated structures.

3. Illustration and Proof for the Substructure Identification Method

Previously proposed substructure methods in the time domain for structural condition assessment always assume a set of well-known boundary conditions. In the application, there are two cases of assumptions for the application. In the first case, the boundary is assumed to be rigid. In this case, the term $\mathbf{F}_{in}$ in Equation (2) is ignored and the equation of motion of the substructure becomes:

$$\mathbf{M}_{ss}\ddot{\mathbf{x}}_s + \mathbf{C}_{ss}\dot{\mathbf{x}}_s + \mathbf{K}_{ss}\mathbf{x}_s = -(\mathbf{MG})_s\ddot{\mathbf{x}}_g + \mathbf{L}_s\mathbf{F}_s \tag{3}$$

In another case, the interaction force of Equation (2) is supposed to be measured. The equation of motion is still as Equation (2) while the term $\mathbf{F}_{in}$ is taken as the constant time history. Otherwise, Equation (3) cannot be used directly.

Assuming the damage extent of the *i*th element in the target substructure is represented as a reduction factor, α_i, the change in the global stiffness matrix of each substructure, can be described as:

$$\Delta\mathbf{K} = \sum_{i}^{Ne} \alpha_i \mathbf{K}_i \tag{4}$$

where *Ne* denotes the number of finite elements of the target substructure. The unknown vector of the structural parameters to be identified is defined as $\boldsymbol{\alpha} = [\alpha_1\ \alpha_2, \ldots\ \alpha_{Ne}]^t$. Based on the two assumptions above and performing differentiation on both sides of the equation of motion for the two cases above with respect to the structural parameters α_i, the equation can be obtained as follows:

$$\mathbf{M}_{ss}\frac{\partial\ddot{\mathbf{x}}_s}{\partial\alpha_i} + \mathbf{C}_{ss}\frac{\partial\dot{\mathbf{x}}_s}{\partial\alpha_i} + \mathbf{K}_{ss}\frac{\partial\mathbf{x}_s}{\partial\alpha_i} = -\frac{\partial\mathbf{K}_{ss}}{\partial\alpha_i}\mathbf{x}_s - a_2\frac{\partial\mathbf{K}_{ss}}{\partial\alpha_i}\dot{\mathbf{x}}_s \tag{5}$$

The responses $\ddot{\mathbf{x}}$, $\dot{\mathbf{x}}$, and $\mathbf{x}$ are obtained by the step-by-step time integration method from Equation (2). They are then substituted into Equation (5). The matrices $\partial\ddot{\mathbf{x}}_s/\partial\alpha_i$, $\partial\dot{\mathbf{x}}_s/\partial\alpha_i$, $\partial\mathbf{x}_s/\partial\alpha_i$ can then be solved similarly by the step-by-step time integration Newmark-β method from Equation (5). The local damage of the structure can be detected with different optimization tools.

However, in structures with isolation, the boundary conditions for the substructures are not as ideal as the two cases mentioned above. In the structure with isolation, the change in the structural parameter may have a large influence on the time history of the interface force of the substructure. When the interaction force changes with the parameters of the target substructure, the methods for the special cases shown above are not applicable for the condition evaluation as shown in this section below. In this general case, the interface force $\mathbf{F}_{in}$ in Equation (2) is known to be a function of the structural parameters α_i. Equation (6) is obtained after applying differentiation with respect to the structural parameter α_i to both sides of Equation (2):

$$\mathbf{M}_{ss}\frac{\partial \ddot{\mathbf{x}}_s}{\partial \alpha_i} + \mathbf{C}_{ss}\frac{\partial \dot{\mathbf{x}}_s}{\partial \alpha_i} + \mathbf{K}_{ss}\frac{\partial \mathbf{x}_s}{\partial \alpha_i} = -\frac{\partial \mathbf{K}_{ss}}{\partial \alpha_i}\mathbf{x}_s - a_2\frac{\partial \mathbf{K}_{ss}}{\partial \alpha_i}\dot{\mathbf{x}}_s + \frac{\partial \mathbf{F}_{in}}{\partial \alpha_i} \tag{6}$$

Equation (6) is different from Equation (5), with an extra term of $\partial \mathbf{F}_{in}/\partial \alpha_i$ at the end of the equation. The matrices $\partial \ddot{\mathbf{x}}_s/\partial \alpha_i$, $\partial \dot{\mathbf{x}}_s/\partial \alpha_i$, $\partial \mathbf{x}_s/\partial \alpha_i$, and $\partial \mathbf{F}_{in}/\partial \alpha_i$ are coupled with respect to α_i and they are difficult to obtain.

A solution to Equation (6) is illustrated and proved in this section. With this solution, the matrices of $\partial \ddot{\mathbf{x}}_s/\partial \alpha_i$, $\partial \dot{\mathbf{x}}_s/\partial \alpha_i$, $\partial \mathbf{x}_s/\partial \alpha_i$ can also be calculated with Equation (5) but with a different physical meaning. The proof is provided below. In this general case, the information required is just the initial model of the target substructure, the insufficient measured acceleration response on the target substructure, and the time history of the earthquake excitation. It is noted that each substructure shown in Figure 1 can be taken as the target substructure and the substructure above the isolation system shown in Figure 2 is just for illustration.

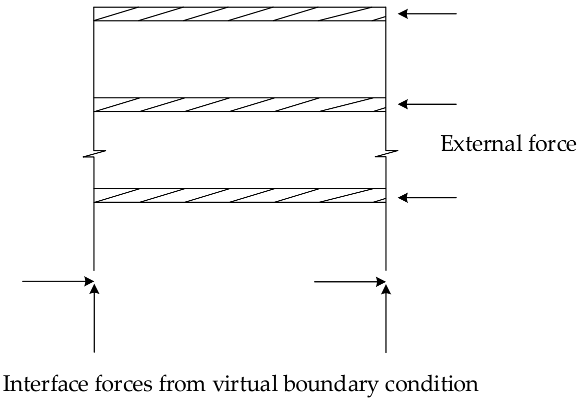

Figure 2. Illustration of the pseudo substructure.

Proof. The solution of $\partial \ddot{\mathbf{x}}_s/\partial \alpha_i$, $\partial \dot{\mathbf{x}}_s/\partial \alpha_i$, $\partial \mathbf{x}_s/\partial \alpha_i$ is based on the construction of a pseudo substructure system with virtual boundary conditions and iterative model updating of the pseudo substructure. The pseudo substructure system illustrated in Figure 2 consists of the target substructures in the initial state with the interface forces from the virtual boundary conditions. It is assumed that in this system, the virtual boundary conditions act as virtual actuators, which can supply the force the same as the interface force of the target substructure in real conditions with local damage under the effect of earthquake excitation. Therefore, the pseudo system is subject to external forces $\mathbf{F}_{real}$, including the interface forces from the virtual boundary condition and the external excitation forces, which are identical to those of the real target substructure with local damages. The response of the pseudo substructure in the kth updating iteration, z_k, can be represented as:

$$\begin{aligned} &\mathbf{z}_k = f(\mathbf{F}_{real}, \boldsymbol{\alpha}_k)\ (k = 1, 2, 3, \ldots) \\ &\boldsymbol{\alpha}_1 = 0 \end{aligned} \tag{7}$$

Since $\mathbf{F}_{real}$ is a set of external force time history from the damaged target substructure, the external forces $\mathbf{F}_{real}$ will not change in the subsequent computational iterations of the pseudo substructure. The response of the pseudo substructure in the updating can, therefore, be represented as:

$$\begin{aligned} &\mathbf{z}_k = f(\boldsymbol{\alpha}_k)\ (k = 1, 2, 3, \ldots) \\ &\boldsymbol{\alpha}_1 = 0 \end{aligned} \tag{8}$$

The equation of motion of the pseudo structural system can, therefore, be represented by Equation (9) as:

$$\mathbf{M}_{ss}\ddot{\mathbf{x}}_s + \mathbf{C}_{ss}\dot{\mathbf{x}}_s + \mathbf{K}_{ss}\mathbf{x}_s = -(\mathbf{MG})_s\ddot{\mathbf{x}}_g + \mathbf{L}_s\mathbf{F}_s + \mathbf{F}_{real} \tag{9}$$

where the subscript real denotes the interface forces corresponding to the damage state of the target substructure, and it is not a function of the stiffness reduction factor α_i in the iteration process. Hence, differentiation is performed on both sides of Equation (9). Equation (5) can be obtained for the pseudo substructure and Equation (5) is applicable for identifying the response sensitivity matrices. It is noted that the solution to Equation (9) is equal to the solution to Equation (2) only when the real substructure and the pseudo substructure have the same damage, including the extent and location. Thus, the model updating of the pseudo substructure is equivalent to the model updating of the real target substructure. This method is proved.

In the following simulation study, the "measure" response, $\ddot{\mathbf{x}}_m$, is obtained as the solution of the equation of motion in Equation (2) from the finite element model with local damages. Taking acceleration as the measured information, the Taylor series expansion on the difference between the "measured" response and the calculated response can be represented as:

$$\ddot{\mathbf{x}}_m - \ddot{\mathbf{x}} = \frac{\partial \ddot{\mathbf{x}}}{\partial \boldsymbol{\alpha}} \cdot \boldsymbol{\alpha} + o(\boldsymbol{\alpha}^2) \tag{10}$$

where $\ddot{\mathbf{x}}$ is the calculated response from the equation of motion of the pseudo substructure system. The stiffness reduction vector $\boldsymbol{\alpha}$ can be calculated from Equation (10) with an optimization method as shown in [32–34]. □

4. The Computation Algorithm

Nonlinear base isolations are often installed at the base or inter-storey of smart structures to reduce the effect of earthquakes. The interface forces for the target substructure, which can be on or under the isolation system, may be difficult to measure or calculate. The present study takes both the interface forces and the local damages of the structure as unknowns in the identification process. In the seismic condition assessment process, two new computational strategies are adopted for substructure condition assessment, which are illustrated in this section.

4.1. Identification of the Interface Forces in the First Stage

The equation of motion of the substructure can be expressed in the state space as:

$$\dot{\mathbf{z}} = \mathbf{A}^C z + \mathbf{B}^C(-\mathbf{MG}\ddot{\mathbf{x}}_g + \mathbf{L}\cdot\mathbf{F}) \tag{11}$$

where $\mathbf{z} = \begin{bmatrix} \mathbf{x} \\ \dot{\mathbf{x}} \end{bmatrix}$, $\mathbf{A}^C = \begin{bmatrix} 0 & \mathbf{I} \\ -\mathbf{M}^{-1}\mathbf{K} & -\mathbf{M}^{-1}\mathbf{C} \end{bmatrix}$ and $\mathbf{B}^C = \begin{bmatrix} 0 \\ \mathbf{M}^{-1} \end{bmatrix}$.

Where $\mathbf{F}$ is the vector of the external excitation forces and the interface forces. The superscript C denotes the matrices of the continuous structural system. Vector $\mathbf{y}(t) \in \mathbf{R}^{ns\times 1}$ represents the observation vector of the output of the structural system and it can be expressed as a combination of acceleration, velocity, and displacement measurements as:

$$\mathbf{y} = \mathbf{R}_a\ddot{\mathbf{x}} + \mathbf{R}_v\dot{\mathbf{x}} + \mathbf{R}_d\mathbf{x} \tag{12}$$

with $\mathbf{R}_a$, $\mathbf{R}_v$, and $\mathbf{R}_d \in \mathbf{R}^{m\times Ndof}$, which are the output influence matrices for the measured acceleration, velocity, and displacement, respectively; m is the dimension of the measured responses; and $Ndof$ is the number of DOFs of the structure. It is shown in Equation (12) that just incomplete measurements are required. Equation (12) can be rewritten as:

$$\mathbf{y} = \mathbf{Rz} + \mathbf{D}\cdot(-\mathbf{M}\ddot{x}_g + \mathbf{L}\cdot\mathbf{F}) \tag{13}$$

where $\mathbf{R} = [\mathbf{R}_d - \mathbf{R}_a\mathbf{M}^{-1}\mathbf{K} \quad \mathbf{R}_v - \mathbf{R}_a\mathbf{M}^{-1}\mathbf{C}]$ and $\mathbf{D} = \mathbf{R}_a\mathbf{M}^{-1}$.

Equations (12) and (13) can be converted into the following discrete equations as:

$$\mathbf{z}(j+1) = \mathbf{A}^{\mathrm{D}}\mathbf{z}(j) + \mathbf{B}^{\mathrm{D}}\cdot(-\mathbf{MG}\ddot{\mathbf{x}}_g + \mathbf{L}\cdot\mathbf{F}(j)) \tag{14}$$

$$\mathbf{y}(j) = \mathbf{Rz}(j) + \mathbf{D}\cdot(-\mathbf{M}\ddot{\mathbf{x}}_g + \mathbf{L}\cdot\mathbf{F}(j)) \quad (j = 1, 2, \cdots, N) \tag{15}$$

where superscript D denotes that the matrices are for the discrete structural system. N is the total number of sampling points and dt is the time step between the state variables $\mathbf{z}(j)$ and $\mathbf{z}(j+1)$ and $\mathbf{A}^{\mathrm{D}} = \exp(\mathbf{A}^{\mathrm{C}}\cdot dt)$, $\mathbf{B}^{\mathrm{D}} = (\mathbf{A}^{\mathrm{C}})^{-1}(\mathbf{A}^{\mathrm{D}} - \mathbf{I})\mathbf{B}^{\mathrm{C}}$. The output $\mathbf{y}(j)$ can be expressed in terms of the previous input $\mathbf{F}(k)$, $(k = 0,\ 1,\ \cdots, j)$ and $\ddot{\mathbf{x}}_g$ with zero initial responses from Equations (15) and (16) as follows:

$$\mathbf{y}(j) = \sum_{k=0}^{j}\mathbf{H}_k\cdot(-\mathbf{MG}\ddot{\mathbf{x}}_g(j-k) + \mathbf{L}\cdot\mathbf{F}(j-k)) \tag{16}$$

where $\mathbf{H}_0 = \mathbf{D}$ and $\mathbf{H}_k = \mathbf{R}(\mathbf{A}^{\mathrm{D}})^{k-1}\mathbf{B}$.

The constants in matrix $\mathbf{H}_k$ in Equation (17) are the system Markov parameters and they are commonly used for the identification of linear dynamic systems [5]. Equation (16) can be rewritten as:

$$\mathbf{Y} - \mathbf{H}_G\ddot{\mathbf{x}}_g = \mathbf{H}_L\mathbf{F} \tag{17}$$

where $\mathbf{H}_L = \begin{bmatrix} \mathbf{H}_0 & 0 & \cdots & 0 \\ \mathbf{H}_1 & \mathbf{H}_0 & \cdots & 0 \\ \vdots & \vdots & \ddots & 0 \\ \mathbf{H}_{N-1} & \mathbf{H}_{N-2} & \cdots & \mathbf{H}_0 \end{bmatrix}\mathbf{L}_S$, $\mathbf{L}_S = \begin{bmatrix} \mathbf{L} & 0 & \cdots & 0 \\ 0 & \mathbf{L} & \cdots & 0 \\ \vdots & \vdots & \ddots & 0 \\ 0 & 0 & \cdots & \mathbf{L} \end{bmatrix}$

$$\mathbf{H}_G = \begin{bmatrix} \mathbf{H}_0 & 0 & \cdots & 0 \\ \mathbf{H}_1 & \mathbf{H}_0 & \cdots & 0 \\ \vdots & \vdots & \ddots & 0 \\ \mathbf{H}_{N-1} & \mathbf{H}_{N-2} & \cdots & \mathbf{H}_0 \end{bmatrix}\mathbf{G}_S,\ \mathbf{G}_S = \begin{bmatrix} -\mathbf{MG} & 0 & \cdots & 0 \\ 0 & -\mathbf{MG} & \cdots & 0 \\ \vdots & \vdots & \ddots & 0 \\ 0 & 0 & \cdots & -\mathbf{MG} \end{bmatrix}$$

$$\mathbf{Y} = \left\{\mathbf{y}(0)^T \quad \mathbf{y}(1)^T \quad \cdots \quad \mathbf{y}(N-1)^T\right\}^T, \mathbf{F} = \left\{\mathbf{F}(0)^T \quad \mathbf{F}(1)^T \quad \cdots \quad \mathbf{F}(N-1)^T\right\}^T.$$

Where matrix $\mathbf{H}_L$ is constant for a system, and the response vector $\mathbf{Y}$ can be obtained from the measured responses. The identification equation for the vector of forces can be written in least-squares sense as:

$$\mathbf{F} = ({\mathbf{H}_L}^T\mathbf{H}_L)^{-1}{\mathbf{H}_L}^T(\mathbf{Y} - \mathbf{H}_G\ddot{\mathbf{x}}_g) \tag{18}$$

The regularization method provides an improved solution to the ill-posed problem in Equation (18), and the damped least-squares method [33–35] is adopted to give bounds to the problem. Equation (19) shows the application of the regularization method in force identification as:

$$\begin{aligned} {\mathbf{H}_L}^T(\mathbf{Y} - \mathbf{H}_G\ddot{\mathbf{x}}_g) &= ({\mathbf{H}_L}^T\mathbf{H}_L + \lambda\mathbf{I})\mathbf{F} \\ \mathbf{F} &= ({\mathbf{H}_L}^T\mathbf{H}_L + \lambda\mathbf{I})^{-1}{\mathbf{H}_L}^T(\mathbf{Y} - \mathbf{H}_G\ddot{\mathbf{x}}_g) \end{aligned} \tag{19}$$

where λ is the non-negative damping coefficient governing the participation of the least-squares error in the solution. Solving Equation (19) is equivalent to minimizing the function:

$$J(F,\lambda) = \left\|\mathbf{H}_L\mathbf{F} - (\mathbf{Y} - \mathbf{H}_G\ddot{\mathbf{x}}_g)\right\|^2 + \lambda\left\|\mathbf{F}\right\|^2 \tag{20}$$

The L-curve method [32] is adopted to find the optimal regularization parameter λ. The intact FEM of the structure is considered in the first iteration and the updated FEM of the structure is used in the subsequent iterations for the force identification [35]. With the identified forces, the response of the structure can be calculated from Equation (9). The local damages can be identified with the adaptive regularization method in the second stage of the general response sensitivity method.

4.2. New Strategies with the First-Stage Identification

4.2.1. Sub-Time Zone Force Identification

The size of matrix $\mathbf{H}_L$ is proportional to the number of sampling points in the measured data and unknowns in the time history of forces. Calculation with a large-sized $\mathbf{H}_L$ is time consuming and can cause delay in the computation with online structural health monitoring. The size of matrix $\mathbf{H}_L$ is proportional to the discrete points in the time history of the external force. Therefore, a reduction in the unknown discrete points in the time history of the external force can improve the computation time.

A sub-time zone force identification procedure is proposed in this section for a more efficient calculation. The measured data are divided into several non-overlapping sub-time zones and the time history of the unknown external forces is identified in each time segment. The initial responses in each segment are calculated from the identified forces of the previous segment at the last sampling point with Equation (2). Hence, the only unknowns in each segment of the external force are the force time history. With the proposed method, the interface forces in each sub-time zone are identified separately in the first stage while in the second stage, the local damage is identified with the complete measured response time history.

4.2.2. Non-Zero Initial Response in Identification

It is very common that the initial responses of the structure are unknown in practice, and the non-zero initial values affect the results of the structural condition assessment based on the structural response in the time domain. When the initial response of the structure is not zero, the time history of the responses of a structure is a function of the initial state, external forces, and structural parameters. The response vector can, therefore, be represented as:

$$\mathbf{Y} = f(\mathbf{Y}_0, \mathbf{F}, \boldsymbol{\alpha}) \tag{21}$$

where $\mathbf{Y}_0$ is the initial state of the structural system. When the structural system is linear, the responses of the structure can be considered as the summation of free vibration due to the non-zero initial responses and the forced vibration due to external excitations. Equation (21) can be rewritten as:

$$\mathbf{Y}=\mathbf{Y}_{\text{fr}}+\mathbf{Y}_{\text{fo}}=g(\mathbf{Y}_0, \boldsymbol{\alpha}) + h(\mathbf{F}, \boldsymbol{\alpha}) \tag{22}$$

where $\mathbf{Y}_{\text{fr}} = g(\mathbf{Y}_0, \boldsymbol{\alpha})$ and $\mathbf{Y}_{\text{fo}} = h(\mathbf{F}, \boldsymbol{\alpha})$ are, respectively, the responses of free vibration and forced vibration.

Considering the free vibration only, the initial response of the structure can be represented as the summation of all mode shapes of the structure as:

$$\mathbf{Y}_0=\begin{bmatrix} \boldsymbol{\Phi} & 0 \\ 0 & \boldsymbol{\Phi} \end{bmatrix}\boldsymbol{\beta} \tag{23}$$

where $\boldsymbol{\Phi}$ is the normalized mode shape matrix of the structure and $\boldsymbol{\beta}$ is a $(2 \times Ndof) \times 1$ vector of contribution coefficients for the vibration modes to be identified. Matrix $\mathbf{Y}_0$ has the dimensions $(2 \times Ndof) \times (2 \times Ndof)$. The total response due to free vibration and forced vibration of the structure can be represented as:

$$\mathbf{Y} = \mathbf{Y}_{\text{ini}} \begin{bmatrix} \mathbf{\Phi} & 0 \\ 0 & \mathbf{\Phi} \end{bmatrix} \boldsymbol{\beta} + \mathbf{H}_L \mathbf{F} \tag{24}$$

where $\mathbf{Y}_{\text{ini}}$ is the free vibration response vector of the structure with one set of mode shapes as the initial state of the structural response at all DOFs of the system. Equation (24) can be written as:

$$\mathbf{Y} = \begin{bmatrix} \mathbf{Y}_{\text{ini}} \begin{bmatrix} \mathbf{\Phi} & 0 \\ 0 & \mathbf{\Phi} \end{bmatrix} & \mathbf{H}_L \end{bmatrix} \begin{bmatrix} \boldsymbol{\beta} \\ \mathbf{F} \end{bmatrix} \tag{25}$$

It is noted that the last vector in Equation (25) consists of the unknown force coefficients and the coefficient vector $\boldsymbol{\beta}$ on the initial response of the system and it can be obtained by a regularization method similar to Equation (20).

4.3. Damage Detection with the Regularization Method

Iterative regularization methods are usually adopted in practical inverse problems, such as load identification, model updating, and damage detection. The objective function in the problem of damage detection in Equation (10), with the Tikhonov regularization method is defined as:

$$J(\Delta \boldsymbol{\alpha}^{k+1}, \lambda) = \left\| \mathbf{S}^k \Delta \boldsymbol{\alpha}^{k+1} - \Delta \ddot{\mathbf{x}}^k \right\|^2 + \lambda^2 \left\| \Delta \alpha^{k+1} \right\|^2 \tag{26}$$

where $\mathbf{S}$ is the sensitivity matrix calculated from Equation (5) and k denotes the kth iteration of the identification and $\Delta\alpha^k$ is the change in the parameter in the kth iteration.

The inverse problem is always ill-posed and measurement noise may have an adverse effect in the process of identification. The iterative identification methods should be able to ensure the significance of the structural parameters and mitigate the unfavorable effect of noise in the identification. An adaptive regularization method has been proposed with an adaptive upper limit on the identified damage determined based on the results from the last iteration step. The objective function of optimization in damage detection is expressed as:

$$J(\Delta \boldsymbol{\alpha}^{k+1}, \lambda) = \left\| \mathbf{S}^k \Delta \boldsymbol{\alpha}^{k+1} - \Delta \ddot{\mathbf{x}}^k \right\| + \lambda^2 \left\| \sum_{i=1}^{k+1} \Delta \boldsymbol{\alpha}^i - \boldsymbol{\alpha}^{k,*} \right\| \tag{27}$$

where $\boldsymbol{\alpha}^{k,*}$ is a value used to coordinate the constraint of the solution in the ith iteration in the damage detection process. Parameter $\boldsymbol{\alpha}^{k,*}$ can be defined as:

$$(\alpha^{k,*})_j = \begin{cases} 0 & \text{if } (\sum\limits_{i=1}^{k} \Delta\alpha^k)_j > 0 \\ (\sum\limits_{i=1}^{k} \Delta\alpha^k)_j & \text{if } (\sum\limits_{i=1}^{k} \Delta\alpha^k)_j < 0 \end{cases} \tag{28}$$

where the subscript j denotes the jth element of the target structure. $(\sum\limits_{i=1}^{k} \Delta\alpha^k)_j$ is the cumulative identified change in the stiffness. The local damage can then be detected iteratively with the obtained optimal parameter λ as:

$$\begin{aligned} &\Delta \boldsymbol{\alpha}^{k+1} = \left(\left(\frac{\partial \ddot{\mathbf{x}}}{\partial \boldsymbol{\alpha}^k} \right)^T \frac{\partial \ddot{\mathbf{x}}}{\partial \boldsymbol{\alpha}^k} + \lambda^2 \mathbf{I}_\alpha \right)^{-1} \left(\frac{\partial \ddot{\mathbf{x}}}{\partial \boldsymbol{\alpha}^k} \right)^T (\ddot{\mathbf{x}}_m^k - \ddot{\mathbf{x}}^k) \\ &\boldsymbol{\alpha}_{k+1} = \boldsymbol{\alpha}_k + \Delta \boldsymbol{\alpha}^k \end{aligned} \tag{29}$$

At the end of the condition assessment, the pseudo substructure should have been updated such that the interface forces and the FEM are updated identically to those of the real damage state of the structure. It should be noted that the force applied by the isolation device is taken as the external excitation; so, this method can be used for both linear or nonlinear isolation layers applied in buildings.

5. The Computation Algorithm

Step 1: Obtain the mass, damping, and stiffness matrices of the target substructure only.

Step 2: Construct the pseudo substructure system.

Step 3: Conduct measurement on the target substructure.

Step 4: Identify the interface forces of the pseudo substructure with the intact model of the pseudo substructure in the state space using Equation (19).

Step 5: Compute the responses of the pseudo substructure with the intact finite element model from Equation (9) with the identified interface forces.

Step 6: Calculate the response sensitivities with respect to the stiffness reduction factor α_n of the substructure $\partial\ddot{x}_i/\partial\alpha_n$, $\partial\dot{x}_i/\partial\alpha_n$ and $\partial x_i/\partial\alpha_n$ from Equation (5).

Step 7: Calculate the local changes in the parameters α_n of the pseudo substructure from Equation (29) with the sensitivity matrix calculated in Step 6.

Step 8: Update the FEM of the pseudo substructure system.

Step 9: Repeat Steps 4 to 7 if the following convergence criteria are not met. Otherwise, stop the computation.

The convergence criteria are defined as:

$$\left\| \frac{\Delta\alpha_{k+1} - \Delta\alpha_k}{\Delta\alpha_{k+1}} \right\| \leq Tol \tag{30}$$

where k denotes the number of iterations and Tol is a small prescribed value, which is 10^{-6} for all studies in this work.

6. Numerical Simulation Studies

A fifteen-storey planar shear frame structure with nonlinear base isolations as shown in Figure 3 was investigated to illustrate the improved two-stage identification method. The structure was subjected to the N-S El-Centro 1940 earthquake ground motion with the peak ground acceleration scaled to 0.3g. The vertical stiffness of the base isolation was assumed as infinitely large. For this case, the target substructure is the main structure above the base isolation system. Therefore, in this case, the pseudo substructure consists of the initial model of the main structure shown in Figure 3 and the interface force is the same as the interface force time history of the target substructure in real conditions during the earthquake excitation. It was assumed that the virtual boundary condition acts as the actuator supply interface forces in real conditions. It is noted that the interface force provided from the virtual boundary condition was taken as the unknown to be identified.

The base isolation between the structure and the foundation is represented with a bilinear hysteresis model. The relationship between the force and horizontal displacement of the base isolation is shown in Figure 4, where α_b = 0.15 is the ratio of the post-yield stiffness to the pre-yield elastic stiffness defined by K_E, and d_y is the yielding displacement. The horizontal restoring force of the isolation is defined as:

$$F_b = \alpha_b K_E x_b + (1 - \alpha_b) K_E z_b \tag{31}$$

where the subscript b denotes the base isolation, x_b is the horizontal deformation of the base isolation, and z_b is the horizontal elastic storey drift between the ground storey and the first storey, K_E = 0.1 × 10^8 N/m and d_y = 0.01 m. The mass of each storey is 4 × 10^5 kg and the stiffness of each storey is 2 × 10^8 N/m.

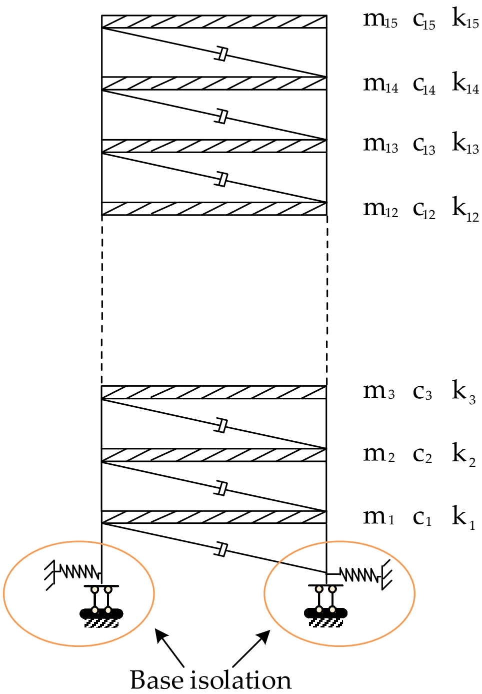

Figure 3. Fifteen-storey shear frame.

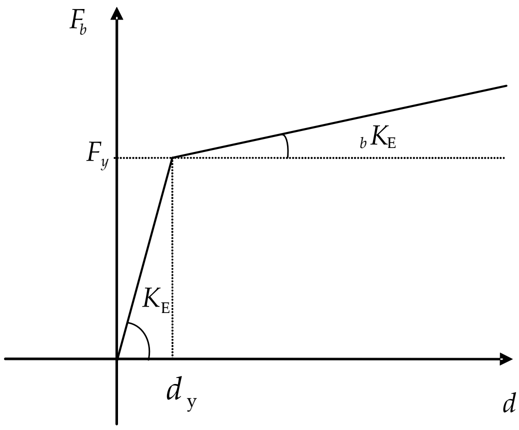

Figure 4. Relationship between force and displacement in the bilinear restoring force model.

The sampling rate of measurement was 100 Hz. Six scenarios with a 10% reduction of stiffness in the 8th storey and 13th storey were studied and are shown in Table 1. The horizontal accelerations at the 1st, 5th, and 10th storeys were taken as the "measured" responses for all six scenarios. Additionally, the horizontal displacement of the first storey was also used in the first stage of force identification in the last two scenarios. This is because the constant value in the time history of the external forces cannot be identified only with acceleration response.

In the first four scenarios, 6 s of "measured" data were used for the condition assessment. The "measured" data for the last two scenarios began at 1.5 s after the earthquake excitation and only 2 s of data were utilized for the initial response identification, interface force identification, and damage detection. The "measured" data was divided into four segments for the sub-time zone force identification in scenarios 3 and 4 while the whole set of data was used for the other scenarios. There was only one interface force at the nonlinear base isolation to be identified in all scenarios.

Table 1. Damage scenarios.

Damage Scenarios	Initial Response	Sub-Time Zone Force Identification	Noise Level (%)
1	zero	No	0
2	zero	No	10
3	zero	Yes	0
4	zero	Yes	10
5	unknown	No	0
6	unknown	No	10

Note that these responses were obtained from computation of the structure under earthquake excitation and the base isolations were performed nonlinearly with the hysteretic curves shown in Figure 5, which demonstrates the bilinear property of the isolation layer. When there was noise in the "measured" response, a polluted response was simulated by adding a normal random component to the "measured" responses as:

$$\ddot{\mathbf{x}}_m = \ddot{\mathbf{x}} + E_P N_{noise} \sigma(\ddot{\mathbf{x}}) \tag{32}$$

where E_P is the percentage noise level, N_{noise} is a standard normal distribution vector with a zero mean and unit standard deviation, and $\sigma(\ddot{\mathbf{x}})$ is the standard deviation of the "measured" acceleration response.

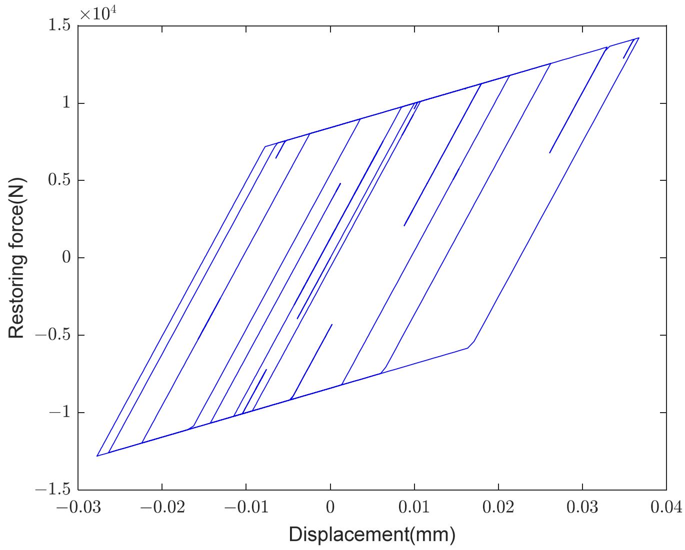

Figure 5. Hysteresis loop of the base isolation.

The error in the identification of the interface forces and the local damages was calculated as:

$$error\,1 = \frac{\|\mathbf{F}_{id} - \mathbf{F}_{true}\|}{\|\mathbf{F}_{true}\|} \times 100\% \tag{33}$$

$$error\,2 = \frac{\|\boldsymbol{\alpha}_{id} - \boldsymbol{\alpha}_{true}\|}{\|\boldsymbol{\alpha}_{true}\|} \times 100\% \tag{34}$$

where $\mathbf{F}_{id}$ and $\boldsymbol{\alpha}_{id}$ are the identified interface forces and local damages, respectively, and $\mathbf{F}_{true}$ and $\boldsymbol{\alpha}_{true}$ are the real interface force and local damages of the substructure, respectively.

In the first two scenarios, the number of unknowns in the first stage was 600 and the measured data was 3×600, which was also the number of equations. The size of matrix $\mathbf{H}_L$ was 1800×600. The number of equations was much larger than the number of unknowns in these two scenarios. In each sub-time zone of the third and fourth scenarios, there were 150 unknowns and 3×150 equations for the interface forces identification. The size of the matrix $\mathbf{H}_L$ in each sub-time zone identification was 450 × 150, which is 1/16th of the size of $\mathbf{H}_L$ in the first two scenarios. In the last two scenarios, the number of unknowns in the first stage was (200 + 2 × 15) = 230 and the number of equations was 4 × 200.

In the second stage of structural condition assessment, there were 15 unknowns in all 6 scenarios. The number of equations was 1800 in the first four scenarios and 600 in the last two scenarios. This shows that the identification problems in this study were all over-determined.

The error of identification for both the interface forces and the local damages and computation time required for each scenario are shown in Table 2 together with the required number of iterations. The results of the damage detection and force identification are shown in Figures 6–11. The stiffnesses shown are the storey stiffnesses of the multi-storey frame.

Table 2. Condition assessment of the six scenarios.

Damage Scenarios	Errors (%)		Calculation Time (s)	Number of Iterations
	Force Identification	Damage Detection		
1	5.55×10^{-3}	8.37×10^{-2}	1493	93
2	13.92	24.04	1511	106
3	9.4×10^{-3}	0.042	94	92
4	14.36	32.97	97	104
5	2.7×10^{-3}	0.03	111	53
6	9.47	62.25	113	58

Figures 6 and 7 show that the two-stage method without measurement noise identified the damage very accurately but with a very long calculation time as shown in Table 2. The calculation of the interface forces is time consuming with a large number of unknowns and a large size matrix $\mathbf{H}_L$. A difference is noted in the peaks of the force time history in Figure 6 when there is 10% measurement noise. However, the position and severity of damage were still accurately identified as shown in Figure 7. The errors in the force identification and damage detection calculated with Equations (33) and (34) are shown in Table 2. It is shown in Table 2 that the measurement noise and accuracy in the identified forces affected the damage detection result.

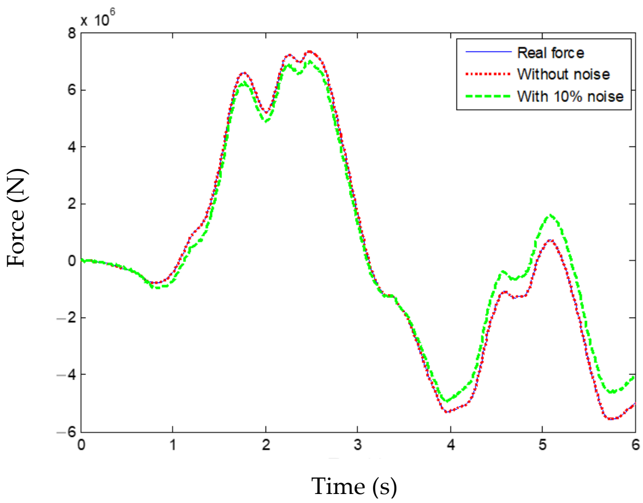

Figure 6. Force identification result (scenarios 1 and 2).

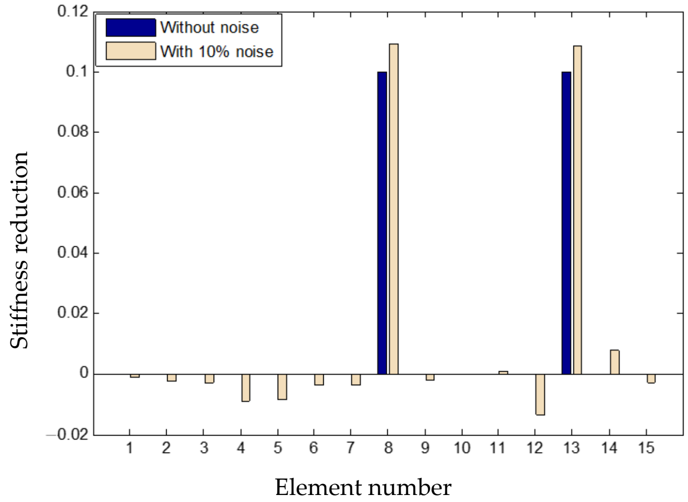

Figure 7. Damage identification result (scenarios 1 and 2).

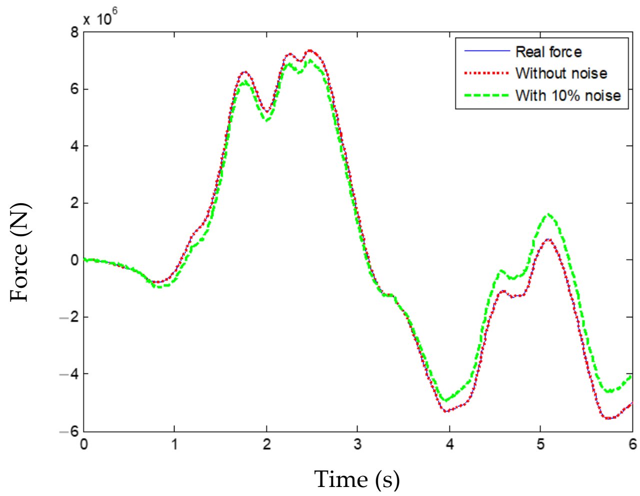

Figure 8. Force identification result (scenarios 3 and 4).

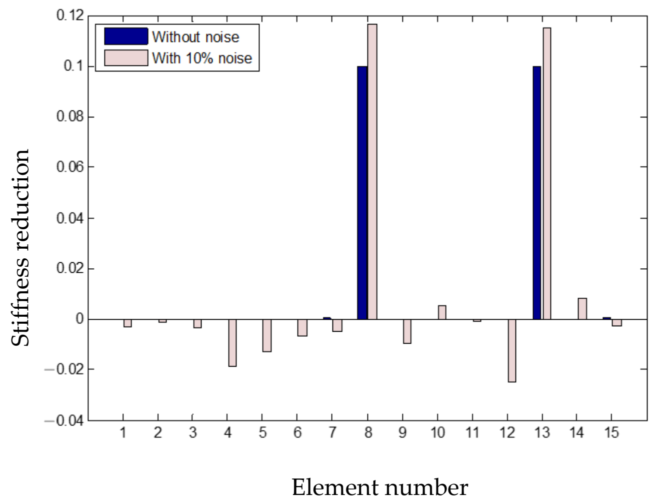

Figure 9. Damage identification result (scenarios 3 and 4).

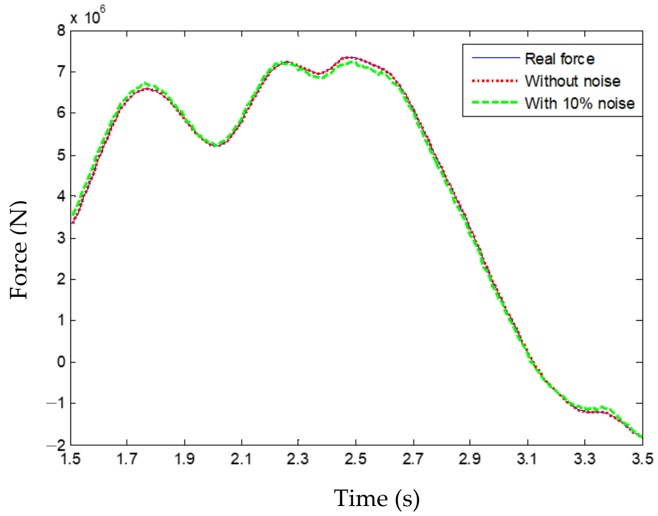

Figure 10. Force identification result (scenarios 5 and 6).

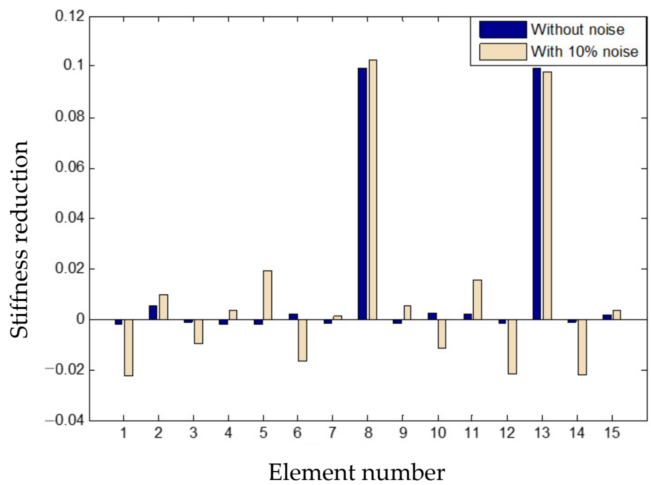

Figure 11. Damage identification result (scenarios 5 and 6).

When the sub-time zone identification method was applied for scenarios 3 and 4, the computation time was reduced significantly as shown in Table 2. The interface force and damage were identified accurately, as shown in Figures 8 and 9, when there was no measurement noise. The errors of identification shown in Table 2 for the identified force are comparable to those from the case that did not use the sub-time zone force identification method. The identified results for the damage are slightly poorer than those for scenarios 1 and 2, but the damage location could still be identified. The cumulative errors in the calculated initial responses in each sub-time zone contribute to the identification error. Mitigation of the cumulative errors will be studied in the future.

The initial responses, the interface forces, and the damage were all identified together in scenarios 5 and 6. The initial responses and the interface forces were identified in the first stage and the local damage was identified in the second stage with the improved two-stage method. Figures 10 and 11 show the identification results without and with 10% measurement noise, respectively. The norm of the damage detection error in Table 2 is large compared with that for scenarios 1 to 4. There is some large error in the damage detection due to both the error of the identification in the initial responses and interface force. However, local damage could still be localized with polluted measurement as shown in Figure 11.

7. Experimental Study

Experimental investigation with a scaled 14-storey concrete shear wall building with an additional 2-storey steel frame on the top connected by isolation was conducted to validate the proposed identification method. The scaled model was constructed on a shaking table with a size of 5 m $\times$ 5 m at the Institute of Engineering Mechanics, China Earthquake Administration, as shown in Figure 12. The geometric scale ratio of the structure was 1/6. Scaled N-S El Centro (1940, NS) earthquake excitation was firstly applied as the base excitation in the y-direction as the main earthquake. The scale ratios of the time and ground acceleration were 0.3 and 1.86, respectively. The details about the scale ratios are shown in Table 3. After this excitation, some damage to the structure may have occurred. A second excitation was applied in the same direction as the aftershock. The structural response excited by the aftershock was measured for the structural model updating and force identification with the proposed method.

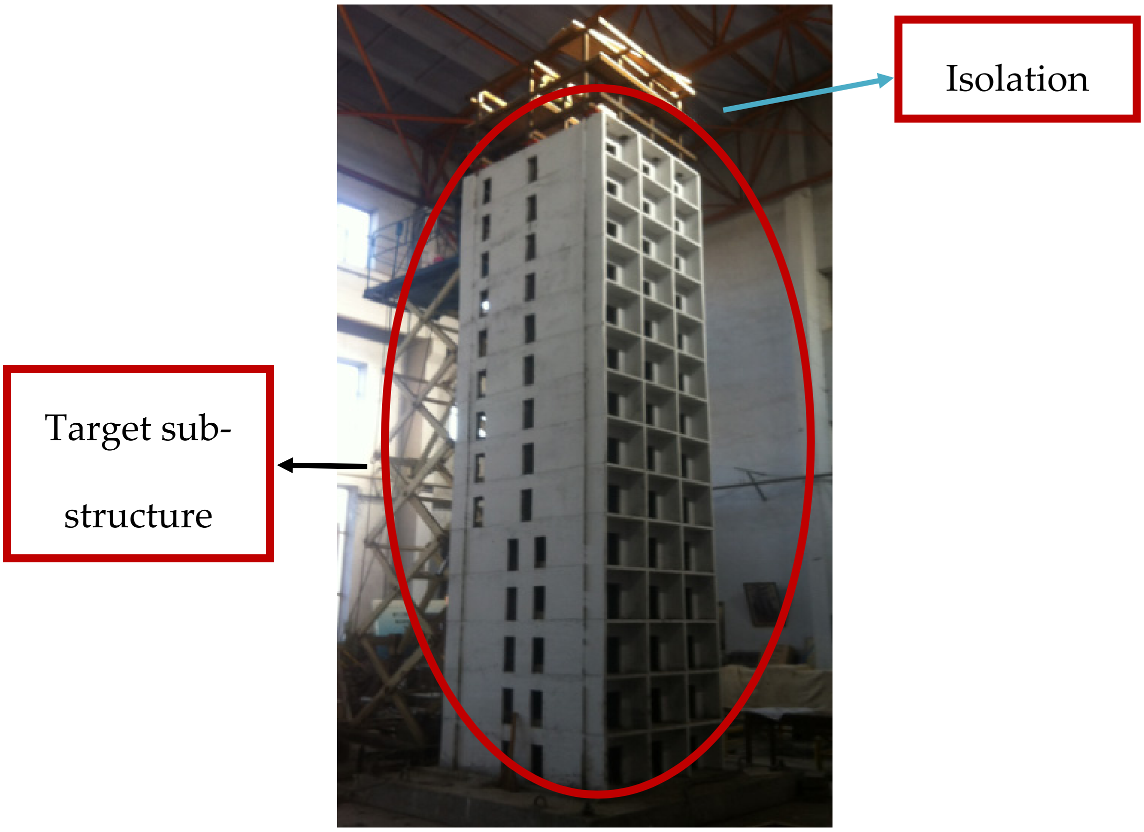

Figure 12. Shear wall building model on the shaking table.

Table 3. Similarity ratio between the model and real structure.

Parameters	Scale Ratio	Parameters	Scale Ratio
Geometric	$S_L = 1{:}6$	Mass	$S_M = S_L{}^2\, S_E/S_a = 1{:}108$
Displacement	$S_X = S_L = 1{:}6$	Time	$S_T = S_L{}^{0.5}/S_a{}^{0.5} = 0.3{:}1$
Stress	$S_F = S_E = 0.62{:}1$	Damping ratio	$S_\xi = 1$
Strain	$S_\varepsilon = 1{:}1$	Acceleration	$S_a = 1.86{:}1$
Young's Modulus	$S_E = 0.62{:}1$	Density	$S_\rho = \frac{S_E}{S_L \cdot S_a} = 2{:}1$

The concrete shear wall building was made from grade M7.5 mortar. The structure was reinforced by a shear wall made from grade M15 mortar outside the original structural and steel wire with an average yielding strength of 852.22 Mpa. The steel wire for the shear wall had the configuration of φ0.8@13 × 13 in the weak direction (x-direction) and φ0.8@13 × 13 in the strong direction (y-direction). Double layers of steel wire mesh were constructed withφ φ0.8@13 × 13 and φ1.9@25 × 25 for the storey plate in the x-direction and y-direction, respectively. The two-storey steel frame structure was fabricated from rectangular steel tubes of grade Q235 with dimensions of 40 mm × 60 mm × 2 mm, and was fixed to the top of the 14-storey shear wall building with bolts through the base plates of the columns. The two-storey steel frame structure was fabricated from 40 mm × 60 mm × 2 mm Q235 rectangular steel tube, and was fixed to the top of the 14-storey shear wall building with rubber isolation. A photograph of the steel frame is shown in Figure 12. Each storey of the steel frame was 483.3 mm high. The column of the frame was welded at the bottom to a base plate, which had 4 Φ20 mm bolt holes to connect the concrete roof of the building and the base isolations were the same as the ones used in [35].

The weight of the whole structural model was 7.62 t and 678 kg additional mass was added on each storey level to simulate the inertia effect of the storey mass. The mass of the structure is mainly found at each storey level, and the 14-storey shear wall building and 2-storey steel frame was simplified into a lumped mass cantilever structure connected with 14 and 2 beam elements, respectively. The two structures were connected with isolation. In the linear condition, the modal properties of the simplified model and the shear wall building structure are compared in Table 4. The accelerometer model 941B made by the Institute of Engineering Mechanics, China Earthquake Administration and the Data Acquisition System model 6000DAS were used in the shaking table test. The sampling rate was 200 Hz and the horizontal accelerations at the 6th, 10th, and 13th storey levels were collected for the storey stiffness identification.

Table 4. Comparison of the natural frequencies of the structure before the main earthquake (Hz).

Modal Order	Experimental Model	Numerical Cantilever Model
1	4.40	4.40
2	10.6	10.6

In this experiment case, the main structure, except the isolation system shown in Figure 12, was divided into two substructures, which are the shear wall concrete structure and steel frame. The two substructures were connected with isolation. The concrete shear wall structure under the isolation system was taken as the target substructure. Hence, in this case, the pseudo substructure consisted of the initial model of the shear wall structure under the isolation and the interface force supplied by the virtual boundary condition. The interface force from the virtual condition was the same as the force time history applied to the concrete shear wall by the isolation system in real conditions during the earthquake excitation. The proposed identification method was applied for the structural model updating. The structural damage identification result is shown in Figure 13. It is shown from the identification result that the structural damage on the lower storeys was larger than the upper storeys after the main earthquake. The largest storey stiffness reduction ratio of nearly 10% was found on the ground storey. The damage on the second storey and third storey was also very large compared with the storeys above. There were some negative stiffness reductions from the 6th to the 10th storey as shown in Figure 13. This is assumed to be the identification errors rather than the real storey stiffness reinforcement.

The comparison of the natural frequencies of the structure after the main earthquake excitation is shown in Table 5. The frequencies from the numerical model were calculated from the updated finite element model with the proposed method in this study and the ones from the experimental model were obtained with white noise excitation. The natural frequencies obtained from the experiment measurement were nearly the same as the calculated value from the updated model. It is demonstrated that the proposed method in this study can identify the structural parameters accurately. It is also shown from the comparison that the frequencies obtained from this experiment are a little bit larger than the numerical ones. This can be explained as some of the cracks may be closed during this low level of white noise excitation. It can be concluded that parameter identification with the structural response during earthquakes is more accurate.

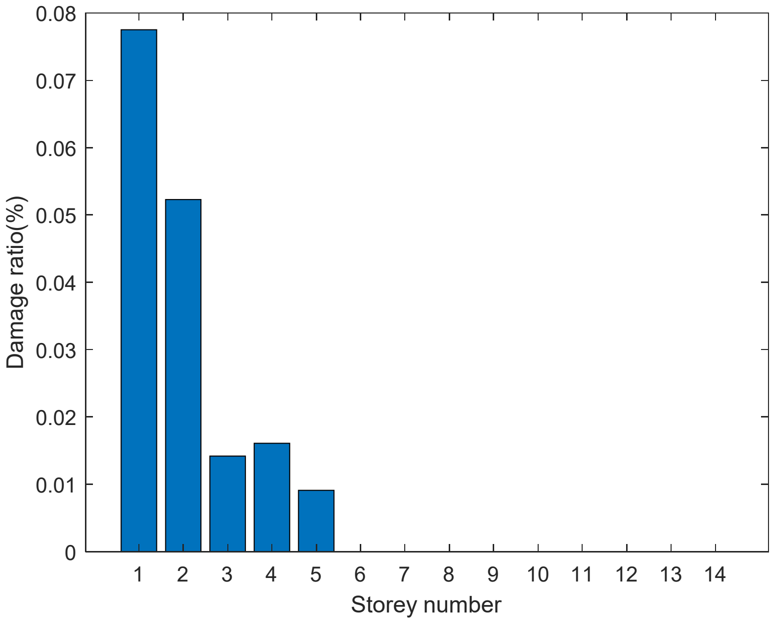

Figure 13. Identified damage ratio of the shear frame.

Table 5. Comparison of the natural frequencies of the structure after the main earthquake (Hz).

Modal Order	Experimental Model	Numerical Cantilever Model
1	4.31	4.27
2	10.52	10.31

8. Conclusions

A seismic damage assessment method for isolation structures based on substructure identification was proposed in this paper. The substructure identification method was proved with the new concept of the pseudo substructure with virtual boundary conditions. The method was modified by considering the calculation efficiency in the first stage of force identification. A sub-time zone method was proposed and implemented to improve the computation efficiency in the force identification. This identification process was also improved by the identification of the unknown initial response. This improvement enables more general applications in engineering practice. The location of damage could be identified fairly accurately with the regularization method and the identified force information. A shaking table test of a 14-storey shear wall structure with a 2-storey steel frame was experimentally investigated to validate the proposed method. It was shown from the experimental study that the structural damage can be detected with acceptable results even there is measurement noise and model error.

Author Contributions: Conceptualization, L.G. and Y.D.; methodology, Y.D.; software, Y.D.; validation, L.G.; formal analysis, L.G.; investigation, L.G.; resources, Y.D.; data curation, L.G.; writing—original draft preparation, Y.D.; writing—review and editing, L.G. and Y.Z.; visualization, Y.Z.; supervision, L.G.; project administration, Y.D.; funding acquisition, Y.D. All authors have read and agreed to the published version of the manuscript.

Funding: This research was funded by Scientific Research Fund of Institute of Engineering Mechanics, China Earthquake Administration (Grant No. 2019D22 and No. 2019D24), Young Talents' Project of

Northeast Agricultural University (18QC31), Projects 2016YFC0701106 of the National Key Research and Development Program of China, No. 51308160 of National Natural Science Foundation of China and open subject of traffic Safety and Control lab in Hebei Province (NO. JTKY2022002).

Institutional Review Board Statement: Not applicable.

Informed Consent Statement: Not applicable.

Conflicts of Interest: The authors declare no conflict of interest.

References

1. Doebling, S.W.; Farrar, C.R.; Prime, M.B. A Summary Review of Vibration-based Damage Identification Methods. *Shock. Vib. Diagn.* **1998**, *30*, 91–105. [CrossRef]
2. Demarie, G.V.; Sabia, D. A machine learning approach for the automatic long-term structural health monitoring. *Struct. Health Monit.* **2019**, *18*, 819–837. [CrossRef]
3. Zou, Y.; Tong, L.; Steven, G.P. Vibration-Based Model-dependent Damage (Delamination) Identification and Health Monitoring for Composite Structure—A Review. *J. Sound Vib.* **1998**, *230*, 357–378. [CrossRef]
4. Nagarajaiah, S.; Basu, B. Output only identification and structural damage detection using time frequency and wavelet techniques. *Earthq. Eng. Eng. Vib.* **2010**, *8*, 583–605. [CrossRef]
5. Juang, J.N. *Applied System Identification*; Prentice Hall: Englewood Cliffs, NJ, USA, 1994.
6. Kumar, V.; Dewangan, H.C.; Sharma, N.; Panda, S.K. Numerical prediction of static and vibration responses of damaged (crack and delamination) laminated shell structure: An experimental verification. *Mech. Syst. Signal Process.* **2022**, *170*, 108883. [CrossRef]
7. Shi, Z.Y.; Law, S.S.; Zhang, L.M. Improved Damage Quantification from Elemental Modal Strain Energy Change. *J. Eng. Mech.* **2002**, *128*, 521–529. [CrossRef]
8. Brincker, R.; Zhang, L.; Andersen, P. Modal Identification of Output-only Systems Using Frequency Domain Decomposition. *Smart Mater. Struct.* **2001**, *10*, 441–445. [CrossRef]
9. Agbabian, M.S.; Masri, S.F.; Caughey, T.K. System Identification Approach to Detection of Structural Changes. *J. Eng. Mech.* **1991**, *117*, 370–390. [CrossRef]
10. Zhu, X.Q.; Law, S.S. Damage Detection in Simply Supported Concrete Bridge Structures under Moving Vehicular Loads. *J. Vib. Acoust.* **2007**, *129*, 58–65. [CrossRef]
11. Lu, Z.R.; Law, S.S. Features of Dynamic Response Sensitivity and Its Application in Damage Identification. *J. Sound Vib.* **2007**, *303*, 305–329. [CrossRef]
12. Law, S.S.; Ding, Y. Substructure Methods for Structural Condition Assessment. *J. Sound Vib.* **2011**, *330*, 3606–3619. [CrossRef]
13. Ding, Y. Structural Control and Condition Assessment with Substructure Method. Ph.D. Thesis, The Hong Kong Polytechnic University, Hong Kong, China, 2012.
14. Jangid, R.; Kelly, J. Base Isolation for Near-fault Motions. *Earthq. Eng. Struct. Dyn.* **2001**, *30*, 691–707. [CrossRef]
15. Erduran, E.; Dao, N.D.; Ryan, K.L. Comparative Response Assessment of Minimally Compliant Low-rise Conventional and Base-isolated Steel Frames. *Earthq. Eng. Struct. Dyn.* **2011**, *40*, 1123–1141. [CrossRef]
16. Pan, P.; Zamfirescu, D.; Nakashima, M.; Nakayasu, N.; Kashiwa, H. Base-isolation Design Practice in Japan: Introduction to the Post-Kobe Approach. *J. Earthq. Eng.* **2005**, *9*, 147–171. [CrossRef]
17. Pant, D.R.; Constantinou, M.C.; Wijeyewickrema, A.C. Re-evaluation of Equivalent Lateral Force Procedure for Prediction of Displacement Demand in Seismically Isolated Structures. *Eng. Struct.* **2013**, *52*, 455–465. [CrossRef]
18. Pharr, G.M. Recent advances in small-scale mechanical property measurement by nanoindentation. *Curr. Opin. Solid State Mater. Sci.* **2015**, *19*, 315–316. [CrossRef]
19. Rossi, E.; Sebastiani, M.; Gigliotti, R.; D'Amato, M. An Innovative Procedure for the In-situ Characterization of Elastomeric Bearings by Using Nanoindentation Test. *Int. J. Archit. Herit.* **2020**, *15*, 79–91. [CrossRef]
20. Hurty, W.C. Dynamic Analysis of Structural. Systems Using Component Modes. *AIAA J.* **1965**, *3*, 678–685. [CrossRef]
21. Yun, C.B.; Lee, H.J. Substructural Identification for Damage Estimation of Structures. *Struct. Saf.* **1997**, *19*, 121–140. [CrossRef]
22. Koh, C.G.; See, L.M.; Balendra, T. Estimation of Structural Parameters in Time Domain: A Substructure Approach. *Earthq. Eng. Struct. Dyn.* **1991**, *20*, 787–801. [CrossRef]
23. Lei, Y.; He, M.Y.; Liu, C.; Lin, S.Z. Identification of Tall Shear Buildings under Unknown Seismic Excitation with Limited Output Measurements. *Adv. Struct. Eng.* **2013**, *77*, 41–52. [CrossRef]
24. Koh, C.G.; Shankar, K. Substructural Identification Method without Interface Measurement. *J. Eng. Mech. ASCE* **2003**, *129*, 769–776. [CrossRef]
25. Zhu, H.P.; Mao, L.; Weng, S. Calculation of Dynamic Response Sensitivity to Substructural Damage Identification under Moving Load. *Adv. Struct. Eng.* **2013**, *16*, 1621–1632. [CrossRef]
26. Guyan, R.J. Reduction of Stiffness and Mass Matrices. *AIAA J.* **1965**, *3*, 380. [CrossRef]
27. Friswell, M.I. Model Reduction Using Dynamic and Iterated IRS. *J. Sound Vib.* **1995**, *186*, 311–323. [CrossRef]

28. Harirchian, E.; Hosseini, S.; Jadhav, K.; Kumari, V.; Rasulzade, S.; Işık, E.; Wasif, M.; Lahmer, T. A Review on Application of Soft Computing Techniques for the Rapid Visual Safety Evaluation and Damage Classification of Existing Buildings. *J. Build. Eng.* **2021**, *43*, 102536. [CrossRef]
29. Valentijn, T.; Margutti, J.; Homberg, M.V.D.; Laaksonen, J. Multi-Hazard and Spatial Transferability of a CNN for Automated Building Damage Assessment. *Remote Sens.* **2020**, *12*, 2839. [CrossRef]
30. Harirchian, E.; Lahmer, T. Improved Rapid Assessment of Earthquake Hazard Safety of Structures via Artificial Neural Networks. *IOP Conf. Ser. Mater. Sci. Eng.* **2020**, *897*, 012014. [CrossRef]
31. Satish, D.; Prakash, E.L.; Anand, K.B. Earthquake vulnerability of city regions based on building typology: Rapid assessment survey. *Asian J. Civ. Eng.* **2021**, *22*, 677–687. [CrossRef]
32. Tikhonov, A.M. On the Solution of Ill-posed Problems and the Method of Regularization. *Sov. Math.* **1963**, *4*, 1035–1038.
33. Li, X.Y.; Law, S.S. Adaptive Tikhonov Regularization for Damage Detection based on Nonlinear Model Updating. *Mech. Syst. Signal Process.* **2010**, *24*, 1646–1664. [CrossRef]
34. Hansen, P.C. Analysis of discrete ill-posed problems by means of the L-curve. *SIAM Rev.* **1992**, *34*, 561–580. [CrossRef]
35. Ding, Y.; Law, S.S.; Wu, B.; Xu, G.S.; Lin, Q.; Jiang, H.B.; Miao, Q.S. Average acceleration discrete algorithm for force identification in state space. *Eng. Struct.* **2013**, *56*, 1880–1892. [CrossRef]